International Journal of Nanomedicine

Dovepress
open access to scientific and medical research

Open Access Full Text Article

ORIGINAL RESEARCH

Application Analysis of ^{124}I-PPMN for Enhanced Retention in Tumors of Prostate Cancer Xenograft Mice

Lei Xia[1,*]
Li Wen[1,2,*]
Xiangxi Meng[1]
Nina Zhou[1]
Xiaoyi Guo[1]
Teli Liu[1]
Xiaoxia Xu[1]
Feng Wang[1]
Hua Zhu[1]
Zhi Yang[1]

[1]Key Laboratory of Carcinogenesis and Translational Research (Ministry of Education/Beijing), NMPA Key Laboratory for Research and Evaluation of Radiopharmaceuticals (National Medical Products Administration), Department of Nuclear Medicine, Peking University Cancer Hospital & Institute, Beijing, 100142, People's Republic of China; [2]Guizhou University School of Medicine, Guiyang, Guizhou, 550025, People's Republic of China

*These authors contributed equally to this work

Correspondence: Hua Zhu; Zhi Yang
Key Laboratory of Carcinogenesis and Translational Research (Ministry of Education/Beijing), NMPA Key Laboratory for Research and Evaluation of Radiopharmaceuticals (National Medical Products Administration), Department of Nuclear Medicine, Peking University Cancer Hospital & Institute, Beijing, 100142, People's Republic of China
Tel +86 010-88196196; +86 010-88196495
Email zhuhuananjing@163.com; pekyz@163.com

Background: In recent years, nuclear medicine imaging and therapy for prostate cancer have radically changed through the introduction of radiolabeled prostate-specific membrane antigen (PSMA)-binding peptides. However, these small molecular probes have some inherent limitations, including high nephrotoxicity and short circulation time, which limits their utility in biological systems.

Methods and Results: In this study, organic melanin nanoparticles were used to directly label the long half-life radionuclide ^{124}I ($t_{1/2}$=100.8 h), and PSMA small molecular groups were efficiently bonded on the surface of nanoparticles to construct the PSMA-targeted long-retention nanoprobe ^{124}I-PPMN, which has the potential to increase tumor uptake and prolong residence time. The results showed that the nanoprobe could substantially aggregate in the tumors of prostate cancer xenograft mice and was visible for more than 72 h. Positron Emission Computed Tomography (PET) imaging showed that the nanoprobe could be used for precise imaging of prostate cancer with high expression of PSMA. In addition, organic melanin nanoparticles labeled with an elemental radionuclide achieved a stable, metal-free structure. Cell experiments and mouse toxicity experiments indicated that the nanoprobe has high safety.

Conclusion: The new nanoprobe constructed in this study has high specificity and biocompatibility. In the future, combined with the multifunctional potential of melanin nanoparticles, this nanoprobe is expected to be used in the integrated theranostics of prostate cancer.

Keywords: prostate cancer, ^{124}I, PET, PSMA, melanin nanoparticles

Instruction

With the steadily aging population worldwide, the incidence and mortality of prostate cancer are increasing over time. It is speculated that the incidence of prostate cancer in the world in 2018 accounted for 13.5% of all cases in high-incidence areas including the United States, Europe, Australia, New Zealand and most parts of sub-Saharan Africa.[1] Early diagnosis and accurate positioning of primary and metastatic lesions can bring better prognosis for patients.[2,3] At present, prostate cancer biopsy is still the most important method for the diagnosis of prostate cancer. Since the 1980s, transrectal ultrasound-guided biopsy (TRUS) has been the gold standard for the diagnosis of prostate cancer. However, this invasive biopsy technique has limitations. There is human subjectivity in biopsy surgery, which cannot avoid the missed diagnosis of some clinically significant cancers caused by high and low technology.[4] On the other hand, templated systematic puncture can lead to the identification of a large number of prostate cancers without

Received: 27 July 2021
Accepted: 29 October 2021
Published: 16 November 2021

clinical significance. At the same time, there may be surgical complications. Although some studies have shown that prostate saturation puncture (approximately 26 needles) can improve the detection rate of prostate cancer, the resulting increase in overdiagnosis and complications is also a problem.[5]

Studies have shown that prostate-specific membrane antigen (PSMA) is highly expressed on the surface of all prostate cancer cells and is an ideal new target for targeted diagnosis and treatment. In recent years, nuclear medicine has undoubtedly been the forefront in the molecular imaging and targeted therapy of prostate cancer.[6,7] Many new cancer-specific molecular probes have been constructed with PSMA as the target. In addition to providing high-sensitivity PET imaging, this approach has achieved good results in the treatment of advanced prostate cancer. Afshar-Oomieh et al[8,9] developed a [^{68}Ga] Ga-PSMA-HBED-CC molecular probe and performed the first PET/CT molecular imaging examination. Subsequently, a variety of novel high-specificity small molecular probes for PSMA were developed and entered clinical translation. While small molecular probes have the advantage of a high clearance rate, they cannot be retained in the long term, which results in a strict imaging time and other disadvantages.[10,11] Nanoparticles have been used as drug carriers for many years, and the drug retention time at the tumor site can be significantly increased through the enhanced permeability and retention (EPR) effect of nanoparticles.[12] The above problems can be solved by relying on nanoparticles as carriers. Moon et al[13] developed a dual-modal PET/MR imaging probe using iron oxide (IO) nanoparticles and a prostate-specific membrane antigen (PSMA)-targeting ligand in aqueous medium. The PSMA small molecule inhibitors used in our study were designed independently based on the latest research.[14] It is challenging for metal-based nanoparticles to achieve clinical applications due to unpredictable toxicity and side effects while needing to maintain high stability.[15]

Melanin is a ubiquitous, amorphous, irregular functional biopolymer in nature. It exists in a variety of biological tissues, including human skin.[16] Organic melanin nanoparticles (MNPs) are constructed from bioderived melanin and exhibit high safety and biocompatibility.[17,18] This type of nanoparticle has been used as a carrier of chemotherapeutic drugs by binding drugs through π-π stacking interactions because of the abundant aromatic rings or hydrogen-bonding groups on its surface.[19] MNPs have controllable particle size, stable structure, good biocompatibility and biodegradability.[20]

Here, our study applied a tumor-targeted nanoplatform to the diagnosis and treatment of prostate cancer (Scheme 1). We changed the structure of PSMA small molecule inhibitors with conserved sites for glutamic acid binding, and the modified area was replaced by mercaptopropionic acid to prepare an active sulfhydryl group. The prostate cancer-targeting nanoprobe PSMA-PEG-MNPs were constructed by chemical methods. The radionuclide ^{124}I was selected for PET imaging. Its long half-life of 100.8 h makes it highly suitable for in vivo monitoring of long-circulating drugs.[21] The novel nanoprobe ^{124}I-PPMN is expected to provide a research basis for prostate cancer-specific theranostics.

Experimental Materials

Preparation and Modification of MNPs

Reference[22] for the preparation methods of multifunctional nanoparticles was optimized and improved. Ultrafine particle size MNPs were prepared by the ultrasonic fragmentation method. Melanin (10 mg) was first dissolved in 3 mL of 0.1 M NaOH solution under intense stirring. Under the action of an ultrasonic cell grinder (15%, 20 W), approximately 2.3 mL of 0.1 M HCl solution was added in one minute, and then, the ultrasonic intensity of the system was gradually increased. The HCl solution was slowly added to reach pH = 7.0, obtaining a black and bright MNPs dispersion. The Na^+ and Cl^- in the solution were removed by ultrafiltration centrifugation with a molecular weight cutoff of 30 kDa, and the purified MNPs were washed twice with deionized water. After freeze-drying, 5 mg of MNPs was fully dispersed in 5 mL of ultrapure water. The pH of the reaction system was adjusted to 9 by 0.1 M NaOH solution, and then, the solution was slowly added to a reaction bottle containing 20 mg NH_2-PEG $_{(5000)}$-NH_2. After stirring for 12 h at room temperature, the unreacted NH_2-PEG $_{(5000)}$-NH_2 was removed by 30 kDa ultrafiltration centrifugation. PEG-MNPs powder was obtained by freeze-drying.

Synthesis and Characterization of PMSA-PEG-MNPs

The amino-sulfhydryl crosslinking agent sulfo-SMCC was used as a linker in the combination of PSMA-SH and NH_2-PEG-MNPs. First, 5 mg of NH_2-PEG-MNPs was fully

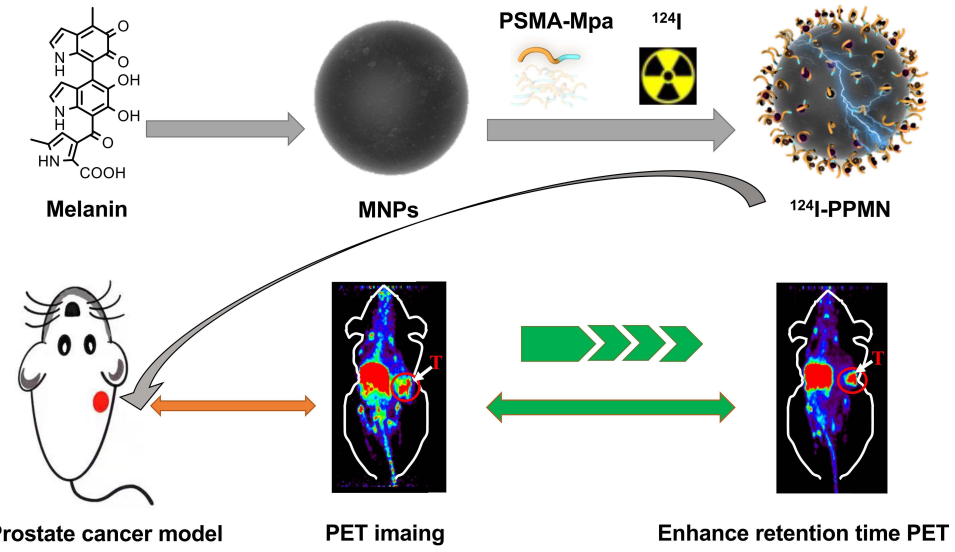

Scheme 1 ^{124}I-PPMN were used to enhanced retention time of PSMA small molecular probe in prostate cancer.

dispersed in 1 mL of ultrapure water, and excess amino-sulfhydryl crosslinking agent sulfo-SMCC (5 μmol) was added and stirred at room temperature for 2 h. Then, the unreacted sulfo-SMCC was separated by a PD-10 column. The reaction solution was concentrated to 0.5 mL by ultrafiltration and slowly added to a solution of PSMA-SH (4 mM, 1 mL). The reaction was stirred overnight at 4 °C. PSMA-PEG-MNPs were purified and collected on a PD-10 column. The morphology of MNPs, PEG-MNPs and PSMA-PEG-MNPs was characterized by transmission electron microscopy (TEM, 200 kV), dynamic light scattering (DLS) particle size analysis, Fourier transform infrared (FTIR) spectroscopy and nuclear magnetic resonance (^{1}H-NMR) spectroscopy.

Synthesis and Characterization of ^{124}I-PPMN

The radionuclide ^{124}I is self-produced by an HM-20 cyclotron. ^{124}I was labeled to PSMA-PEG-MNPs using N-bromosuccinimide (NBS) as an oxidant for the electrophilic substitution reaction. This method refers to an ^{124}I-labeled monoclonal antibody. PSMA-PEG-MNPs (1 mg) were fully dispersed into 500 μL of 0.1 M phosphate buffer (PB) solution, mixed with ^{124}I (500 μCi), and then added to 20 μL of NBS solution. The reaction was immediately timed for 1 min. After 1 min, the solution was then purified by a PD-10 column. Radio-TLC was used for the quality control of radioactive labeling. First, 3 μL of labeling product (0.2 MBq) was dropped to 1 cm below the iTLC-SG silica gel plate, and acetone was used as the expansion solution for ^{124}I-PPMN. Then, 30 μL (1.2 MBq) of the labeled products was added into 200 μL of 0.01 M PBS (pH = 7.4) solution and 200 μL of 5% HSA saline. Radio-TLC detection was performed at 0, 2 h, 12 h, 24 h, 48 h, 72 h and 96 h.

Cell Uptake and Competitive Inhibition of ^{124}I-PPMN

The cellular uptake and inhibitory uptake of ^{124}I-PPMN were tested using LNCaP and PC-3 human prostate cancer cells (these cells were kindly provided by Stem Cell Bank, Chinese Academy of Sciences). LNCaP and PC-3 cells were cultured in complete McCoy's 5A and PRIM1640 medium, respectively, to logarithmic phase. Two groups of cells were placed in 24-well plates, with 2×10^5 cells per well, and then, 500 μL of complete medium was added to each well for 24 h. The ^{124}I-PPMN were diluted to 37 kBq/μL (1 μCi/μL) using sterile PBS (0.01 M, pH = 7.4), 10 μL of nanoprobe was added to each well of cells, and the cells were placed in the incubator again. Two 24-well plates were removed at 2 h, 24 h and 48 h. At each time point, 6 holes of the two cells were taken as a group. After cleaning, 200 μL of NaOH (2.0 M) was added to each hole for cell cleavage. A cell uptake blocking experiment was performed by adding a certain amount of PSMA-SH (2 mg/mL, 10 μL) into the cell orifice plate before adding the same dose of nanoprobe.

PET Imaging and Radioactivity Distribution of ^{124}I-PPMN

In vivo PET imaging was performed on super nova Micro-PET/CT (PINGSENG, China). Free ^{124}I accumulated in the thyroid, and 0.5% potassium iodide (KI) solution was used for thyroid sealing in a mouse model. The ^{124}I-PPMN solution was first filtered through a 0.22 μm organic filter membrane, and 300 μL (11.1 MBq) of nanoprobe was intravenously injected into LNCaP and 22RV1 tumor-bearing mice (these mice were purchased from Beijing Vital River Laboratory Animal Technology Co., Ltd.) (n = 3) via the tail vein. Micro-PET long-term imaging was performed at 2 h, 5 h, 26 h, 48 h and 72 h. At the same time, mice were anesthetized with isoflurane before imaging and maintained anesthesia during imaging (volume factor 1%). Using micro-PET data processing software for region of interest (ROI) delineation, the tumor/nontumor ratio (T/NT) radioactive body distribution diagram was drawn. The SPSS 22.0 (IBM, Chicago, IL, USA) software package was used for statistical analysis. Independent sample t tests were used for statistical analysis. $P < 0.001$ indicated that the difference was statistically significant. All animal experiments were completed in accordance with the relevant guides and regulations of Beijing Cancer Hospital.

Cytotoxicity and Toxicology Experiments in vivo

An MTT assay was used to detect the cytotoxicity of PEG-MNPs and PSMA-PEG-MNPs in vitro with LNCaP and 22RV1 prostate cancer cells. They were cultured to logarithmic phase, digested with trypsin and dispersed into medium without fetal bovine serum. The cells were seeded in 96-well plates at 5000 cells per well and cultured in an incubator for 24 h. Probes diluted to 0.125, 0.25, 0.5, 1 and 2 mg/mL were added to each group and incubated again in an incubator for 24 h. Then, 20 μL MTT of solution (0.5 mg/mL) was added to each well, and the culture was stopped after 3–4 h in the incubator under dark conditions. The supernatant of the orifice plate was carefully removed, and 150 μL of DMSO solution was added to each well. The orifice plate was placed in a shaker at low speed for 10 min and then sent for inspection. The optical absorption value (OD) was recorded at 490 nm by an enzyme-labeled system.

In the ^{124}I-PPMN toxicological experiment, normal 4-week-old male Kunming mice were selected, and 10 mice were randomly divided into two groups with 5 mice in each group, which were marked as the experimental group and the control group. The experimental group was injected with ^{124}I-PPMN via the tail vein (37 MBq/per mouse). Approximately 200 μL of blood was taken from the fundus vein at 1 h, 24 h, 48 h, 192 h and 480 h, and the blood was placed in a collection tube containing sodium citrate solution to avoid blood coagulation. The liver function of 1 h blood samples was immediately detected by an automatic biochemical analyzer, and all blood samples were detected by an automatic blood cell analyzer. The data were collected and statistically analyzed by software, and the differences in parameters between the experimental group and the control group were compared. The mice used in the toxicological experiment were fed for 30 days. Then, one mouse in the experimental group was euthanized for anatomy of the main organs: heart, liver, spleen, lung, kidney and small intestine.

Statistical Analysis

Statistical analyses of the data were performed with SPSS 19.0 software. Measurement data are expressed as the mean ± SD. For cell viability assays and cell uptake, Student's *t* test was applied to identify significant differences. A 95% confidence level was chosen to determine the significance between groups, with a *p value less than 0.05 being significantly different and a ***p value less than 0.001. Multiple group comparisons were conducted by one-way analysis of variance (ANOVA). A value of $*p < 0.05$ was considered statistically significant.

Results and Discussion

Preparation and Characterization of PSMA-SH

The synthetic route of PSMA-SH was based on fully protecting the conserved glutamic acid binding site and the conserved metal (Zn^{2+}) catalytic site of the original PSMA small molecule inhibitor, and the chemical modification was improved to construct an activated hydroxyl group. The synthesis was commissioned by ChinaPeptides Co., Ltd. A small amount of PSMA-SH was fully dissolved in anhydrous acetonitrile for HPLC and ESI-MS detection. According to the HPLC results (Figure S1A), the purity of PSMA-SH was more than 95%, and the peak

time was 10.55 min. The ESI-MS detection results showed that the synthesized PSMA-SH had obvious product peaks at 766.3 ([M+H]+) (Figure S1B), which proved that PSMA-SH was successfully synthesized and that its chemical purity met the requirements of use.

Synthesis and Characterization of ^{124}I-PPMN

Melanin nanoparticles are supramolecular nanoparticles synthesized by the π-π conjugation of natural melanin analogs. A series of improvements have been made on the basis of the original synthesis method. MNPs can be uniformly dispersed in water, which is different from melanin. In addition, the surface of MNPs contains a large number of catechol groups, nitrogen atoms and carboxyl groups, which can efficiently adsorb metal ions. However, the surface properties of nanoparticles will change after adsorbing metal ions or other chemical groups, leading to particle polymerization. The stability of nanoparticles in solution can be greatly improved after modifying diamino polyethylene glycol (PEG) on the surface of MNPs by using a Michael addition reaction.

The synthetic route of ^{124}I-PPMN is shown in Figure S2. TEM, DLS, FT-IR and ^{1}H-NMR analyses were used to evaluate the nanoprobes. High-resolution TEM can clearly show the morphology and structure of nanoparticles. TEM images of MNPs and PSMA-PEG-MNPs are shown in Figures 1A and B. The MNPs were roundish, regular in size and well dispersed in aqueous solution. The core particle size was approximately 6 nm. There was no significant change in the morphology and structure of PSMA-PEG-MNPs after modification. DLS can detect the hydrated particle size of nanoparticles, which is more in line with the actual particle size of nanoparticles in solution. The hydroclynamic sizes of MNPs, PEG-MNPs and PSMA-PEG-MNPs are shown in Figure 1D–F, with the statistics in Table 1. The hydration particle size of MNPs was approximately 6.42 ± 2.10 nm, and the PEG-MNPs reached 8.43 ± 3.16 nm after PEG modification. The hydration particle size of PSMA-PEG-MNPs increased to 13.65 ± 3.65 nm. Table 1 summarizes the hydrodynamic particle size of nanoparticles at different stages. It is noteworthy that the particle size of the final product ^{124}I-PPMN decreased slightly compared with that of the PSMA-PEG-MNPs. This difference may be due to the slight change in the structure of nanoparticles during the labeling process of the ^{124}I radionuclide, but the particle size of 12.73 ± 2.41 nm is still within the optimal particle size range (10–100 nm) for nanoparticle biological applications.[23,24] Small nanoparticles can increase the uptake speed and metabolic rate in tumor sites.

Fourier transform infrared spectroscopy was used to detect the chemical structure changes of the nanoprobes. As shown in Figure 1C, the C–H stretching vibration peak at 2873 cm^{-1} and the C–O–C stretching vibration peak at 1052 cm^{-1} were the characteristic absorption peaks of PEG that appeared in PEG-MNPs. At the same time, the ^{1}H-NMR results further verified the combination of PEG and MNPs (Figure 1H). The MNPs dispersed in D_2O did not exhibit obvious signal peaks in the proton spectrum, which was because most conjugated main chains were buried inside the nanoparticles. The 3.6 ppm signal peak representing PEG ($-OCH_2CH_2O-$) proved that PEG was successfully modified on the surface of MNPs. In addition, the infrared spectrum of PSMA-PEG-MNPs showed a weak C–S single bond peak at 965 cm^{-1}, and the inorganic peak at 518 cm^{-1} was considered to be from a small amount of metal contained in PBS solution. The results of infrared spectroscopy provide reference value for the successful construction of PSMA-PEG-MNPs. After the difference calculation of residual PEG-MNPs, it was obtained that approximately 15 PSMA-SH groups were bound on the surface of PEG-MNPs. X-ray photoelectron spectroscopy (XPS) was used to verify the elemental distribution of I-PSMA-PEG-MNPs. The results showed that the nanoprobe contained a large amount of iodine in addition to the elements in PSMA-PEG-MNPs (Figure 1G).

The Labeling of ^{124}I and Pharmacokinetics of ^{124}I-PPMN

In this study, high-purity ^{124}I was prepared by a ^{124}Te (p, n) ^{124}I reaction using an HM-20 medical cyclotron. The labeling rate of ^{124}I-PPMN was as high as 98%, the radiochemical purity was 99% after purification, and the radiochemical purity remained above 90% within 96 h (Figure 2A). The drug metabolism-time curves of the nanoprobe showed its circulation time in organisms, which provided guidance for drug toxicity analysis and treatment planning. After detection, the pharmacokinetic curves of ^{124}I-PPMN were fitted by Prism 6.0 software, which conformed to the two-compartment model (Figure 2B). The formula was as follows:

$$Ct = A1 * \exp(-\alpha t) + A2 * \exp(-\beta t)$$

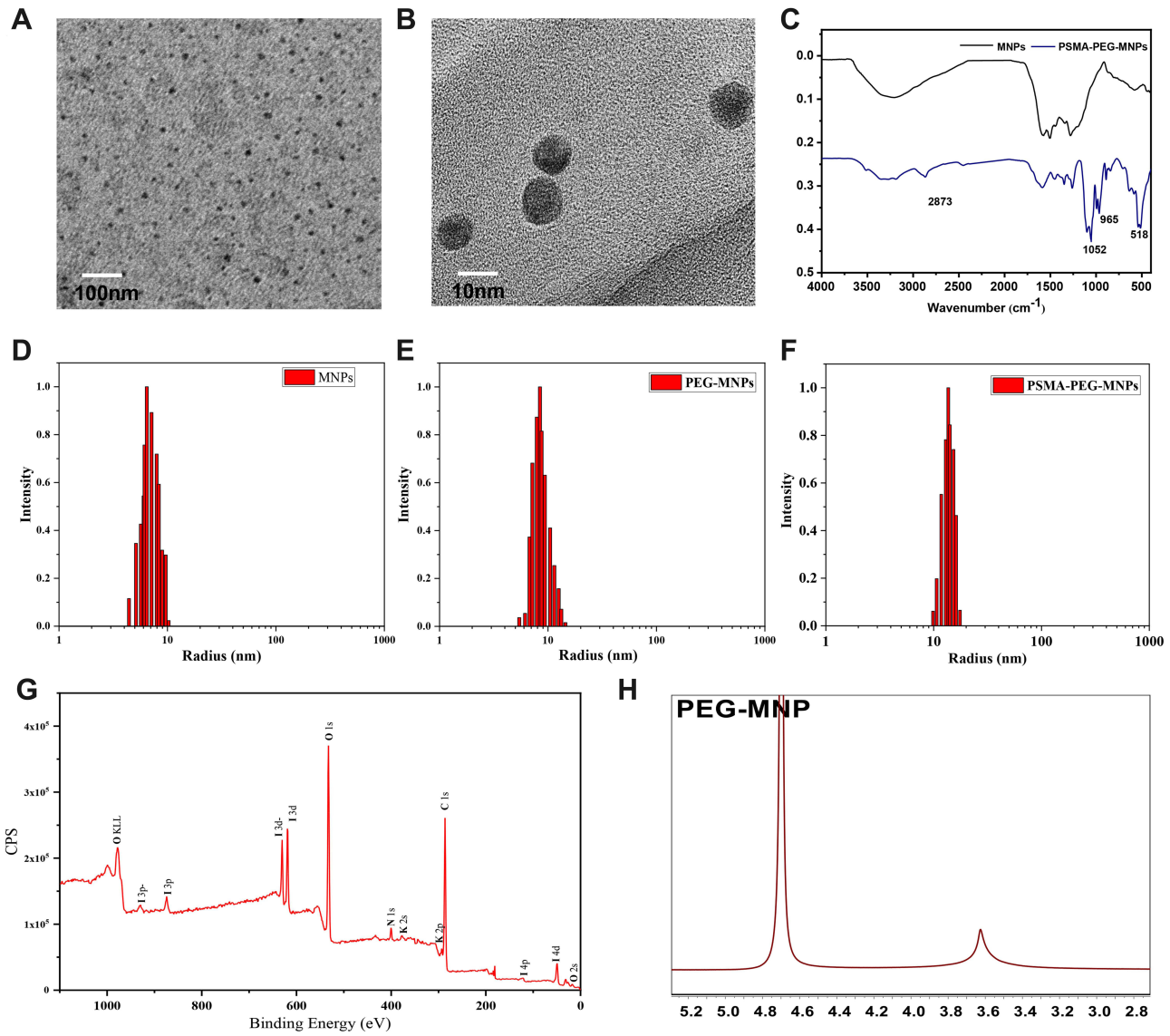

Figure 1 Characterization of the nanoprobe. (**A**) TEM of MNPs (scale bar=100 nm). (**B**) TEM of PSMA-PEG-MNPs (scale bar=10 nm). (**C**) FT-IR spectra of MNPs (black line) and PSMA-PEG-MNPs (blue line) dispersed in aqueous solution. Hydrodynamic size distribution graphs of MNPs (**D**), PEG-MNPs (**E**) and PSMA-PEG-MNPs (**F**). (**G**) XPS of I-PSMA-PEG-MNPs. (**H**) ^{1}H-NMR of PEG-MNPs.

In this model, A1 and A2 are the intercepts of the central chamber and outer chamber with the longitudinal axis, respectively, and α and β are the rate constants of the central chamber and outer chamber, respectively. The data measured by a γ-counter are converted into the formula, and the model formula is Ct = 17.88 * exp (−4.926t) + 5.312 * exp (−0.1417t). The biological half-lives of the distribution phase and scavenging phase of ^{124}I-PSMA-PEG-UMNPs were 0.14 h and 4.8 h, respectively.

Table 1 The Data of Hydrodynamic Sizes of Various Nanoprobe

Nanoprobe	Diameter
MNPs	6.42±2.10 nm
PEG-MNPs	8.43±3.16 nm
PSMA-PEG-MNPs	13.65±3.65 nm
^{124}I-PPMN	12.73±2.41 nm

Cell Uptake and Competitive Inhibition of ^{124}I-PPMN

The specific targeting of ^{124}I-PPMN to the PSMA receptor was verified by the cellular uptake of ^{124}I-PPMN in LNCaP cells with high PSMA expression and PC-3 cells with low PSMA expression. The results showed that the uptake ratios of ^{124}I-PPMN in LNCaP and PC-3 cells were 1.24 ± 0.11% and 0.45 ± 0.08% at 1 h after the

addition of nanoprobes, respectively (Figure 2C). At 4 h, the differences between the two groups were the largest, with uptake ratios of 2.90 ± 0.12% and 0.81 ± 0.15%, respectively. The differences continued until 24 h, and the uptake values of LNCaP and PC-3 cells were 3.37 ± 0.24% and 1.36 ± 0.35%, respectively. The results of cell blocking showed that the uptake ratios of ^{124}I-PPMN without the blocking group and with the blocking group were 3.93 ± 0.22% and 1.22 ± 0.31% at 4 h, respectively (Figure 2D). These results proved the targeting specificity of ^{124}I-PSMA-PEG-MNPs for PSMA-positive cells.

Detection of PSMA Expression in LNCaP and 22RV1 Tumor-Bearing Mice

PSMA is highly expressed in 98% of prostate cancers, and it has become an ideal target for prostate cancer targeted diagnosis and therapy. In this study, LNCaP tumor mice with high expression of PSMA and 22RV1 tumor models with medium-high expression of PSMA were selected for micro-PET imaging. After successful construction of the tumor-bearing mouse model, the expression of PSMA in the tumor model was verified by immunohistochemical staining and Western blot analysis. The immunohistochemical staining patterns of PSMA expression in LNCaP and 22RV1 tumor tissues were

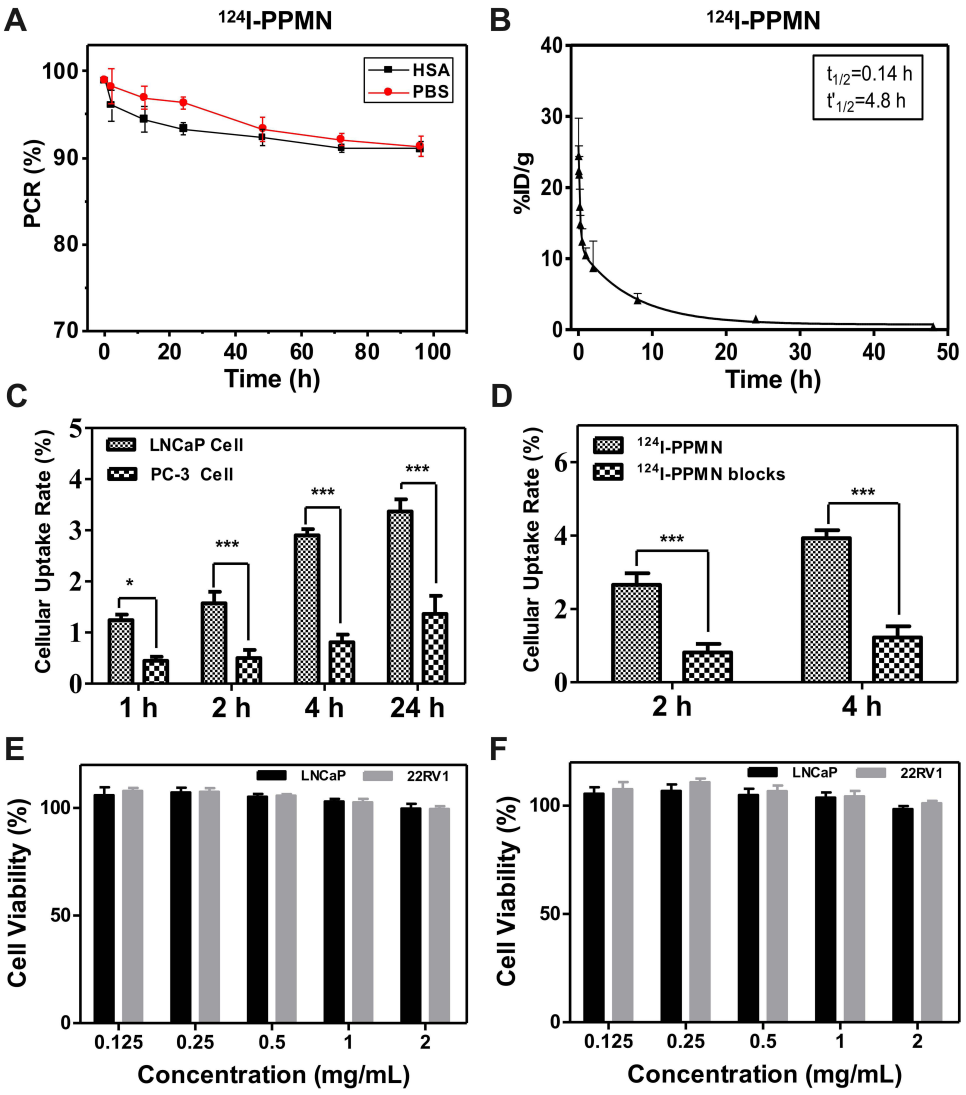

Figure 2 Characterization and safety detection of ^{124}I-PPMN in vitro and in vivo. (**A**) Stability of ^{124}I-PPMN in vitro. (**B**) Blood circulation of ^{124}I-PPMN in vivo. The pharmacokinetics of ^{124}I-PPMN followed the two-compartment model. (**C**) Uptake of ^{124}I-PPMN in LNCaP and PC-3 cells. (**D**) Uptake of ^{124}I-PPMN with and without blocking in LNCaP cells. All of these results are expressed as the mean ± SD. Asterisks indicate *p value < 0.05 and ***p value < 0.001. MTT assay using LNCaP and 22RV1 cells with PEG-MNPs. (**E**) and PSMA-PEG-MNPs. (**F**) concentrations of 0.125, 0.25, 0.5, 1 and 2 mg/mL after 24 h incubation at 37 °C.

significantly different (Figure 3A). The LNCaP tumor staining pattern showed that the cell edge was obviously stained red–brown, while the red–brown color of the 22RV1 tumor cell edge was slight. The Western blot results are shown in Figure 3B. The predicted position of PSMA expression was 80–85 KD, with β-actin protein as the internal reference. The specific band was detected at 84 KD in the LNCaP tumor model, while the specific band at 84 KD in the 22RV1 tumor model was slightly shallow. The gray values of the characteristic bands of the two groups of samples were detected and counted (Figure 3C).

Comparative Detection of ^{124}I-PPMN Micro-PET Imaging

^{124}I-PPMN micro-PET imaging was performed for 72 h after drug injection based on ^{124}I. Figure 4A shows that ^{124}I-PPMN had obvious uptake in the tumor site of the LNCaP model, the radioactivity distribution was mainly concentrated in the heart, liver, spleen, intestine and tumor site at 2 h after injection, and the tumor/nontumor ratio (T/NT) was only 0.77 ± 0.58 (Figure 4C). With prolonged time, the uptake of tumor sites in micro-PET imaging increased gradually. The uptake of tumor sites reached higher values at 5 h, 26 h and 48 h, and the T/NT values were 2.35 ± 0.57, 3.61 ± 0.23 and 4.25 ± 0.37, respectively, which were significantly higher than those at 2 h. At 72 h after drug injection, the uptake of the nanoprobe was still obvious in the tumor site. The ^{124}I-PPMN intake of the 22RV1 tumor site was lower than that of the LNCaP imaging group (Figure 4B), but the nanoprobe remained in the tumor site for more than 72 h. The T/NT values at different time points were significantly different from those of the LNCaP group. All these results prove the high specificity of the nanoprobe in human prostate cancer with high expression of PSMA. The long retention time of the ^{124}I-PPMN in the tumor site was beneficial to adjust the imaging time flexibly, promote the effect of radionuclide targeted therapy and realize long-term imaging monitoring of the therapeutic effect. The radioactivity distribution of ^{124}I-PPMN was mainly in the hepatobiliary system, which was consistent with the metabolic mode of nanoparticles. In addition, its uptake in the intestine was considered to be related to intestinal flora because normal intestinal mucosal cells do not highly express PSMA, but the specific reasons need to be further explored.

Cytotoxicity and Toxicology in vivo

Bioderived organic melanin nanoparticles have inherent biocompatibility. The cytotoxicity test results showed that both PEG-MNPs and PSMA-PEG-MNPs had high cell safety (Figure 2E and F). When the concentration of PEG-MNPs reached 2 mg/mL, the activity of LNCaP cells was still as high as 96.5%, while that of 22RV1 cells was 98.3%. There was no significant difference in cell activity between the two cell lines at different concentrations of PEG-MNPs. The activity of the LNCaP and 22RV1 cell lines reached 95.9% and 97.6%, respectively, with 2 mg/mL PSMA-PEG-MNPs. There was no significant difference in the activity of the two cell lines at different concentrations of PSMA-PEG-MNPs.

The safety of nanoprobes in organisms can be detected through toxicological experiments in vivo. Micro-PET imaging has shown that ^{124}I-PPMN are metabolized through

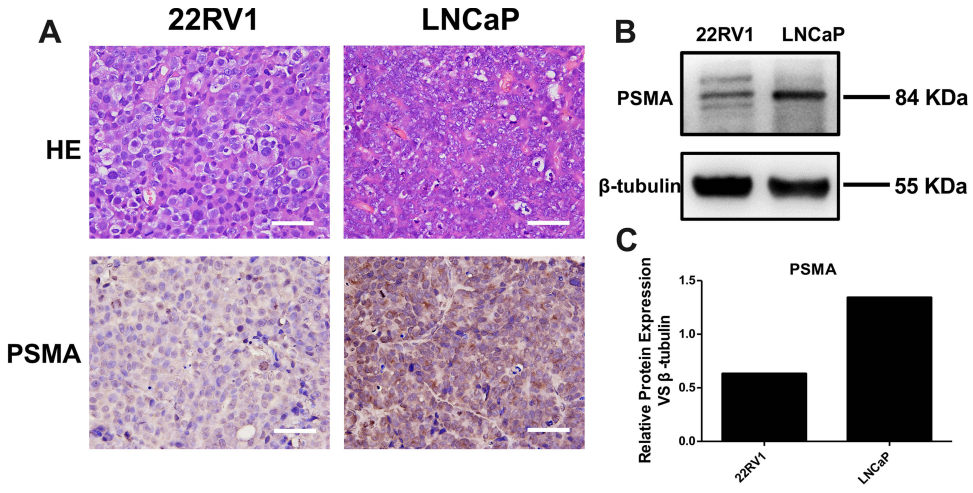

Figure 3 PSMA expression in LNCaP and 22RV1 tumor tissues was measured by immunohistochemical staining and Western blot analysis. (**A**) HE and PSMA staining of 22RV1 (left) and LNCaP (right) tumor tissues. Scale bar = 20 μm. (**B**) Relative PSMA expression in 22RV1 (left column) and LNCaP (right column) tumor tissues. (**C**) Representative PSMA expression is presented as the ratio of PSMA to β-tubulin expression by Western blot analysis. All data were represented as the mean ± SEM (n = 3).

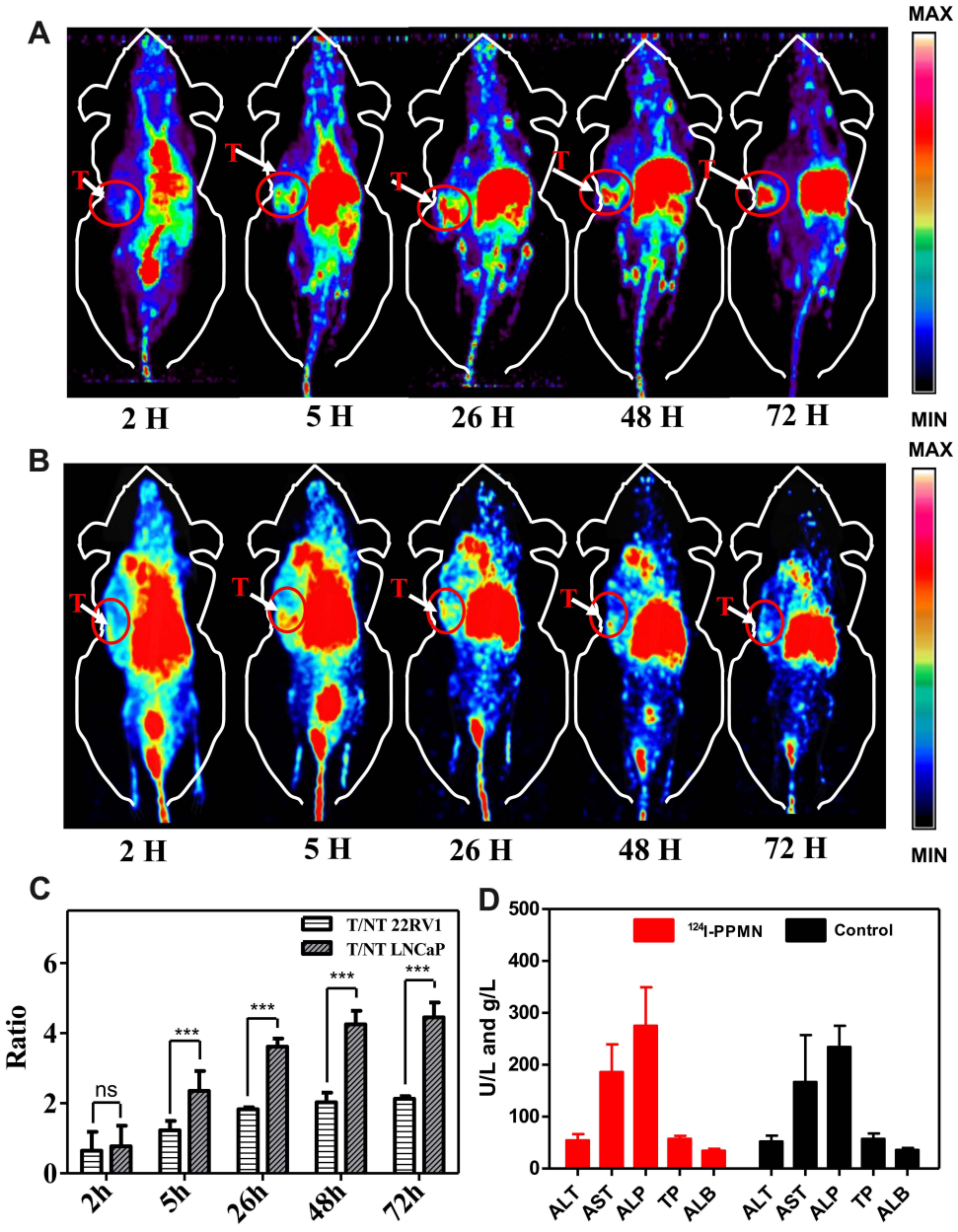

Figure 4 In vivo PET imaging and toxicological detection of ^{124}I-PPMN. (A) Micro-PET images of the LNCaP model (region enveloped by red dotted line) acquired at 2, 5, 26, 48 and 72 h after tail vein injection with ^{124}I-PPMN. (B) Micro-PET images of the 22RV1 model after tail vein injection of ^{124}I-PPMN. (C) The radioactivity distribution of micro-PET images of 22RV1 and LNCaP assessed by T/NT at 2, 5, 26, 48 and 72 h. Asterisk indicates ^{ns}p-value > 0.05 and $^{***}p$-value < 0.001. (D) The blood levels of ALT, AST, ALP, TP, and ALB from treated and healthy control mice.

the liver, so these nanoparticles may cause acute liver injury. The alanine aminotransferase (ALT), aspartate aminotransferase (AST), alkaline phosphatase (ALP), serum total protein (TP) and serum albumin (ALB) levels of mice 2 h after drug injection were detected by liver function blood biochemistry and compared with the control group. As shown in Figure 4D, there was no significant difference in the five indicators between the experimental group and the control group (P > 0.05), and the data of each group were within the normal range (Table S1). It was proved that ^{124}I-PPMN did not cause acute liver injury after tail vein injection in mice. Then, 20 days after injection of ^{124}I-PPMN, the experimental mouse was sacrificed, and important organs, including the heart, liver, spleen, lung, kidney and small intestine, were removed. The organs were fixed and sliced for HE staining. The results showed that no significant histological difference was observed after full comparison of the organ staining images (Figure 5). In

particular, there were no significant changes in the liver and spleen in terms of the main uptake tissue of the nanoprobe. These results showed that the excessive injection of ^{124}I-PPMN did not cause damage to important organs of mice 20 days later.

Conclusion

In summary, a novel nanoprobe, ^{124}I-PPMN, was constructed and characterized by using a melanin nanoplatform, which could be used as a long-retention nanoprobe for prostate cancer targeting PSMA. ^{124}I-PPMN showed good stability and safety in vitro and in vivo. The results verified that application of the nanoprobe for micro-PET imaging of human prostate cancer tumor models showed high sensitivity and reliable targeting to prostate cancer cells. Compared with traditional PSMA-targeted small molecule probes, ^{124}I-PPMN has high specificity and a long retention effect in tumor sites. The construction of ^{124}I-PPMN represents a preliminary exploration of a tumor-specific multimodal platform in this project, and a multimodality theranostic integration nanoprobe for prostate cancer will be further constructed on the basis of this experiment.

Acknowledgements

We thank the cyclotron teams of the Department of Nuclear Medicine, Peking University Cancer Hospital and Institute for ^{124}I production.

Funding

This work was supported, in part, by the National Natural Science Foundation of China (Nos. 81671733 and 81871386), Beijing Municipal Administration of Hospitals-Yangfan Project (ZYLX201816) and Science Foundation of Peking University Cancer Hospital (2021-17).

Disclosure

The authors report no conflicts of interest in this work.

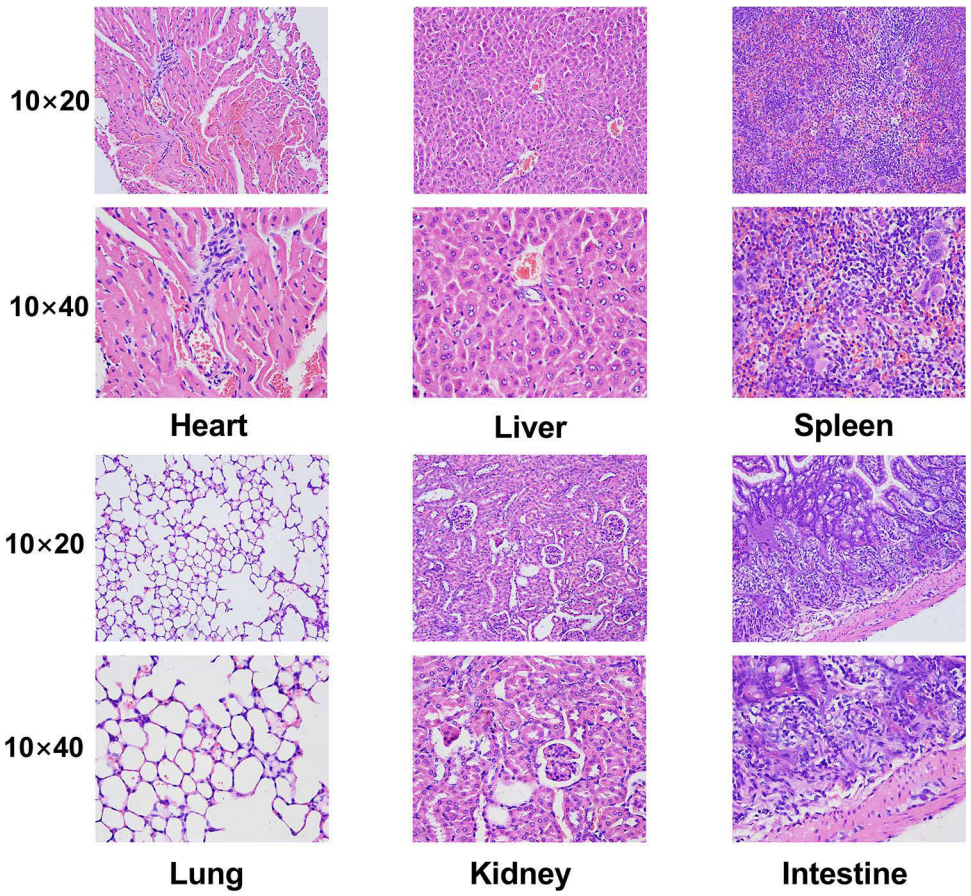

Figure 5 HE staining images of major organs (heart, liver, spleen, lung, kidney and intestine) of the injection group. Scale bars=50 mm.

References

1. Bray F, Ferlay J, Soerjomataram I, et al. Global cancer statistics 2018: GLOBOCAN estimates of incidence and mortality worldwide for 36 cancers in 185 countries. *CA Cancer J Clin*. 2018;68(6):394–424. doi:10.3322/caac.21492
2. Qi D, Wu C, Liu F, et al. Trends of prostate cancer incidence and mortality in Shanghai, China from 1973 to 2009. *Prostate*. 2015;75 (14):1662–1668. doi:10.1002/pros.23046
3. Park BK, Lee HM, Kim CK, et al. Lesion localization in patients with a previous negative transrectal ultrasound biopsy and persistently elevated prostate specific antigen level using diffusion-weighted imaging at three tesla before rebiopsy. *Invest Radiol*. 2008;43 (11):789–793. doi:10.1097/RLI.0b013e318183725e
4. Heck MM, Retz M, Tauber R, et al. PSMA-targeted radioligand therapy in prostate cancer. *Urologe A*. 2017;56(1):32–39. doi:10.1007/s00120-016-0274-3
5. Harvey CJ, Pilcher J, Richenberg J, et al. Applications of transrectal ultrasound in prostate cancer. *Br J Radiol*. 2012;85(Special issue 1): S3–S17. doi:10.1259/bjr/56357549
6. Thompson IM, Chi C, Ankerst DP, et al. Effect of finasteride on the sensitivity of PSA for detecting prostate cancer. *J Natl Cancer Inst*. 2007;25(1):89–90. doi:10.1093/jnci/djj307
7. Muller BG, Shih JH, Sankineni S, et al. Prostate cancer: interobserver agreement and accuracy with the revised prostate imaging reporting and data system at multiparametric MR imaging. *Radiology*. 2015;277(3):741–750. doi:10.1148/radiol.2015142818
8. Afshar-Oromieh A, Holland-Letz T, Giesel FL, et al. Diagnostic performance of 68Ga-PSMA-11 (HBED-CC) PET/CT in patients with recurrent prostate cancer: evaluation in 1007 patients. *Eur J Nucl Med Mol Imaging*. 2017;44(8):1258–1268. doi:10.1007/s00259-017-3711-7
9. Afshar-Oromieh A, Haberkorn U, Eder M, et al. [68Ga]Gallium-labelled PSMA ligand as superior PET tracer for the diagnosis of prostate cancer: comparison with 18F-FECH. *Eur J Nucl Med Mol Imaging*. 2012;39(6):1085–1086. doi:10.1007/s00259-012-2069-0
10. Maresca KP, Hillier SM, Femia FJ, et al. A series of halogenated heterodimeric inhibitors of prostate specific membrane antigen (PSMA) as radiolabeled probes for targeting prostate cancer. *J Med Chem*. 2009;52(2):347–357. doi:10.1021/jm800994j
11. Barrett JA, Coleman RE, Goldsmith SJ, et al. First-in-man evaluation of 2 high-affinity PSMA-avid small molecules for imaging prostate cancer. *J Nucl Med*. 2013;54(3):380–387. doi:10.2967/jnumed.112.111203
12. Xia L, Guo X, Liu T, et al. Multimodality Imaging of Naturally Active Melanin Nanoparticles Targeting Somatostatin Receptor Subtype 2 in Human Small-Cell Lung Cancer. *Nanoscale*. 2019;11:14400–14409. doi:10.1039/C9NR04371C
13. Moon SH, Yang BY, Kim YJ, et al. Development of a complementary PET/MR dual-modal imaging probe for targeting prostate-specific membrane antigen (PSMA). *Nanomedicine*. 2016;12(4):871–879. doi:10.1016/j.nano.2015.12.368
14. Duan X, Liu F, Kwon H, et al. (S)-3-(Carboxyformamido)-2-(3-(carboxymethyl)ureido) propanoic Acid as a Novel PSMA Targeting Scaffold for Prostate Cancer Imaging. *J Med Chem*. 2020;67 (7):3563–3576. doi:10.1021/acs.jmedchem.9b02031
15. Ding L, Liu Z, Aggrey MO, et al. Nanotoxicity: the Toxicity Research Progress of Metal and Metal- Containing Nanoparticles. *Mini Rev Med Chem*. 2015;15(7):529–542. doi:10.2174/1389557515071504241043 34
16. Liu Y, Ai K, Liu J, et al. Dopamine-melanin colloidal nanospheres: an efficient near-infrared photothermal therapeutic agent for In Vivo cancer therapy. *Adv Mater*. 2013;25(9):1353–1359. doi:10.1002/adma.201204683
17. Xia L, Meng X, Wen L, et al. A Highly Specific Multiple Enhancement Theranostic Nanoprobe for PET/MRI/PAI Image-Guided Radioisotope Combined Photothermal Therapy in Prostate Cancer. *Small*. 2021;17(21):e2100378. doi:10.1002/smll.202100378
18. Xia L, Cheng Z, Zhu H, et al. Preparation and Preliminary Molecular Imaging Study of 124I in-situ Labeled Organic Melanin Nanoparticles. *ACTA CHIMICA SINICA*. 2019;77:172–178. doi:10.6023/A18090410
19. Ings RM. The melanin binding of drugs and its implications. *Drug MetabRev*. 1984;15(5–6):1183–1212. doi:10.3109/03602538409033561
20. Sun Y, Hong S, Ma X, et al. Recyclable Cu(i)/melanin dots for cycloaddition, bioconjugation and cell labelling. *Chem Sci*. 2016;7 (9):5888–5892. doi:10.1039/C6SC01536K
21. Lubberink M, Herzog H. Quantitative imaging of 124I and 86Y with PET. *Eur J Nucl Med Mol Imaging*. 2011;38:S10–8. doi:10.1007/s00259-011-1768-2
22. Fan Q, Cheng K, Hu X, et al. Transferring Biomarker into Molecular Probe: melanin Nanoparticle as a Naturally Active Platform for Multimodality Imaging. *J Am Chem Soc*. 2014;136(43):15185–15194. doi:10.1021/ja505412p
23. Hoshyar N, Gray S, Han H, et al. The effect of nanoparticle size on in vivo pharmacokinetics and cellular interaction. *Nanomedicine*. 2016;11(6):673–692. doi:10.2217/nnm.16.5
24. Simon JD, Hong L, Peles DN. Insights into melanosomes and melanin from some interesting spatial and temporal properties. *J Phys Chem B*. 2008;112(42):13201–13217. doi:10.1021/jp804248h